J Mater Sci (2007) 42:7286–7293
DOI 10.1007/s10853-007-1546-5

Effect of in situ spinel seeding on synthesis of MgO-rich $MgAl_2O_4$ composite

Deepak Mohapatra · Debasish Sarkar

Received: 19 September 2006 / Accepted: 23 January 2007 / Published online: 10 May 2007

Abstract MgO-rich $MgAl_2O_4$ spinel was prepared by adopting solid-state reaction of commercially available sintered seawater magnesia and α-alumina. Starting materials were mixed in weight ratio (Al_2O_3: MgO) of 1:1, 1:1.1, 1:1.2, 1:1.3, 1:1.4, where the developed $MgAl_2O_4$ spinel crystal seed in calcined powder varied (5–50%) with respect to addition of MgO content and temperature. Around 70% spinellisation could be noticed in Al_2O_3: MgO (1:1) batch through double stage sintering. Densification and grain size of the sintered specimen was found to be greatly dependent on initial calcination temperature and content of primary spinel seed. The diametrical compressive strength of sintered specimen was ~115 MPa for highest amount of spinel content. The hardness of MgO-rich spinel composite was varied with spinel addition.

Introduction

People of cement industry are affected by allergic skin ulceration and certain respiratory diseases because of the carcinogenic effect of Cr^{6+}, which originate from oxidation of Cr^{3+} in magnesite-chrome and/or chrome–magnesite refractories [1, 2]. In this context, Gonsalves and Maschio et al. investigated $MgAl_2O_4$ spinel and MgO-spinel based refractories for a large number of applications as an alternative component of chrome-containing refractory [3, 4]. But, the direct sintering of $MgAl_2O_4$ from their constituent oxides is very difficult because of the 5–7% volume expansion. Consequently, a two stage firing process has been employed, where first one is to complete the spinel formation and the second one is sintering at an optimum temperature to densify the formed spinel. Among this group of materials, the MgO-rich $MgAl_2O_4$ composites have significant importance for various applications, and detailed study have been carried out by different schools. Bailey et al. found that excess magnesia is beneficial for densification of spinel and 95% theoretical density could be achieved through double-stage sintering, where the periclase controls the grain boundary motion and helps producing dense, small grained body with superior mechanical characteristics [5]. Pasquier et al. proposed in their seminal work that a crystallographic seeding can stabilize a particular phase at higher temperature or lower the crystallization temperature, and/or to enhance the densification. The orderness, i.e., [311] phase of $MgAl_2O_4$ spinel could be increased with addition of 1.69 wt.% $MgAl_2O_4$ spinel seed and this also enhanced the percentage of spinel at low temperature when processed through chemical route [6]. J. Xiaolin reveals 1% crystal seeds are beneficial for the synthesis of fully crystallized $MgAl_2O_4$ spinel through sol-gel route, where initial temperature has been maintained at about 550 °C and crystallization of $MgAl_2O_4$ spinel could be noticed at a temperature of about 700 °C [7]. Ghosh et al. also worked out on the seeding effect on synthesis of MgO-rich spinel. They also reported that incorporation of 20 wt.% $MgAl_2O_4$ spinel in production of MgO refractory has great influence in improving the lower mechanical/thermo-mechanical properties [8]. Working on the development of magnesia–magnesium aluminate co-clinker, Cooper and Hudson found MgO–$MgAl_2O_4$ bricks with 40 wt.% spinel co-clinker resulted in best combination of properties superior resistance against thermal shock

D. Mohapatra · D. Sarkar (✉)
Department of Ceramic Engineering,
National Institute of Technology, Rourkela 8 Orissa, India
e-mail: dsarkar@nitrkl.ac.in

damage and possible erosion and corrosion. Recently, Aksel et al. illustrates that the bending strength of MgO-spinel composite is ~160 MPa, which has been prepared with the addition of 5 wt.% of spinel powder and sintered at 1,650 °C through hot pressing method [9]. The author also found that the 3-pt bending strength decreased uniformly with increasing additions of spinel, and with increasing spinel particle size. However, Simonov observed the compressive strength of the preiclase and MgO-spinel materials within the range of 25–80 MPa [10]. Cunbing et al. observed an increasing trend of hardness for transparent spinel ceramics with increasing alumina content, whereas a discontinuous trend could be noticed for flexural strength measurement [11].

By paying close attention to the earlier research work, it is well understood that the crystallization behavior and densification of MgO-rich spinel depend on the amount of initial MgO-phase content, amount of spinel seed and/or temperature. However, the effects of in-situ spinel seed content through solid-state reaction of MgO-rich $MgAl_2O_4$ spinel on crystallization and densification behavior are limited. In the present work, a wide range of MgO-rich spinel was prepared from their constituent solid-oxides through calcination at different temperatures. Phase analysis and densification were carried out of the sintered specimens. The sintered MgO-rich spinels were characterized and analyzed for the crystallization behavior, extent of spinel phase development and microstructure. Finally an attempt was made to correlate the effect of spinel seed addition on the crystallization behavior, microstructure and mechanical properties of sintered speciemens.

Experimental

Seawater magnesia and commercially available α-Al_2O_3 (NALCO, INDIA) were used as starting materials. Different batches, with weight proportion of Al_2O_3: xMgO, where x = 1, 1.1, 1.2, 1.3, 1.4 were mixed. Calcination of the different batch powders was carried out at different temperatures ranging from 1,000 °C to 1,300 °C with 100 °C temperature interval for 2 h soaking at peak temperature. The powders were milled with the help of high dense ZrO_2 balls in acetone media. The phases in the mixed, calcined and sintered samples were analyzed using an X-ray diffractometer (Phillips PW1830, Netherlands; using Cu-Kα radiation). The crystallite size 't' was determined from X-ray line broadening using the Scherer formula

$$t = 0.9\lambda/B\cos\theta, \tag{1}$$

where 't' is the crystallite size, B (2θ) is the broadening of the diffraction line measured at half maximum intensity, λ is the wavelength of the X-ray radiation, and θ is the Bragg's angle. Line broadening due to the equipment was subtracted from the peak width before calculating the crystallite size using the following formula, $B^2 = B^2_{meas} - B^2_{Equip}$, where, B_{meas} = measured full width at half maximum from peak values, B_{Inst} = Instrumental broadening.

The spinel content in the calcined as well as sintered samples was calculated from the XRD analysis using the Eq. 2 [12].

$$\%\ \text{of}\ MgAl_2O_4 = \left\{ \frac{\text{Height counts of}\ MgAl_2O_{4\{311\}}}{\sum \text{Height counts}\ (MgAl_2O_{4\{311\}} + MgO_{\{200\}} + Al_2O_{3\{104\}})} \right\} * 100 \tag{2}$$

The lattice parameter was calculated [13] from

$$a = \frac{\lambda}{2\,\text{Sin}\,\theta}\sqrt{(h^2 + k^2 + l^2)} \tag{3}$$

where, 'a' is lattice parameter, λ is radiation wavelength and 'h' 'k' 'l' are corresponding Miller indices. For the study of densification behavior of the calcined powders, pellets of 12 mm diameter were prepared by uniaxial pressing at ~275 MPa using 2 wt.% poly vinyl alcohol (PVA) as organic binder. The pellets were heated at a rate of 5 °C/min. The densification study was carried out in a high temperature dilatometer (NETZSCH DL 402C) without any isothermal treatment. The green pellets were prepared from powder calcined at different temperatures and followed by sintering in ambient atmosphere at 1,600 °C for 4 h. Densification study of the sintered products was performed by the conventional liquid displacement method using Archimedes' Principle in Kerosene medium. Microstructure of the polished and thermally etched samples was observed under Scanning Electron Microscope (FEI QUANTA, The Netherlands). The sintered specimens were taken for mechanical properties measurement. The strength of the sintered pellets was measured by standard Brazilian disk test [14]. The sintered compacts were placed diametrically in between two compressing grips and tested for their strength with

the cross-head speed of 0.3 mm min^{-1}. The compressive strength of circular pellets was measured using the formula:

$$\sigma_c = \frac{2P}{\pi DT} \quad (4)$$

Five specimens were tested to obtain a mean value, using a Universal Testing Machine (Hounsfield H10 KS). The hardness of compacts was estimated by Universal Vickers Hardness tester with a load of 98N [15]. Furthermore, the detail hardness calculation was studied by Zeiss Optical Microscope.

Results and discussion

Figure 1 represents the XRD pattern of calcined powders synthesized from their constituent oxides at different temperatures. At lower temperature, all the powder exhibits broader XRD peaks of $MgAl_2O_4$ spinel phase, in addition with minor peak of unreacted corundum and sharp peaks of excess periclase phase (Fig. 1a). The crystallization of $MgAl_2O_4$ is observed at 1,000 °C, which is well agreed with the earlier research work [16]. Figure 1b reveals the trend of unreacted corundum phase, which is less in case of higher calcination temperature. Table 1 shows the calculated vol% of $MgAl_2O_4$ formation after calcination at different temperatures. At 1,000 °C, 5–6 vol% spinel phase could be observed, whereas ~30 vol% spinel content was noticed for highest MgO content. The detailed phase analysis of calcined powder illustrates a gradual trend of increasing spinel formation with increasing calcination temperature as well as increasing MgO content. The phase analysis of XRD peak demonstrates ~28 and ~48 vol% spinel phase develops at 1,300 °C for the lowest and highest MgO content respectively. Figure 1a evidences initiation of spinel phase with broad lines, which reveals the crystallinity at this temperature is low. With increase in calcination temperature (1,000–1,300 °C) the diffraction peaks of spinel became sharper due to increase in the crystallinity of spinel phase (Fig. 1b). The measured crystal size for samples calcined at different temperature is listed in Table 2. The crystallite size is 19 nm for lowest calcination temperature and lowest content of MgO. However, the crystallite size gradually increases with increasing temperature and maximum 33 nm has been detected for MAP5 powder at 1,300 °C for 2 h. The calculated average lattice parameter (a_o = 8.0792 Å) of $MgAl_2O_4$ with highest MgO content has highest value. This may be due to the enlargement of spinel unit cell structure with the formation of oxygen vacant sites i.e., spinel structure becomes anion deficient due to excess MgO [17]. The results also indicate that $MgAl_2O_4$ spinel phase develops with increasing calcination temperature.

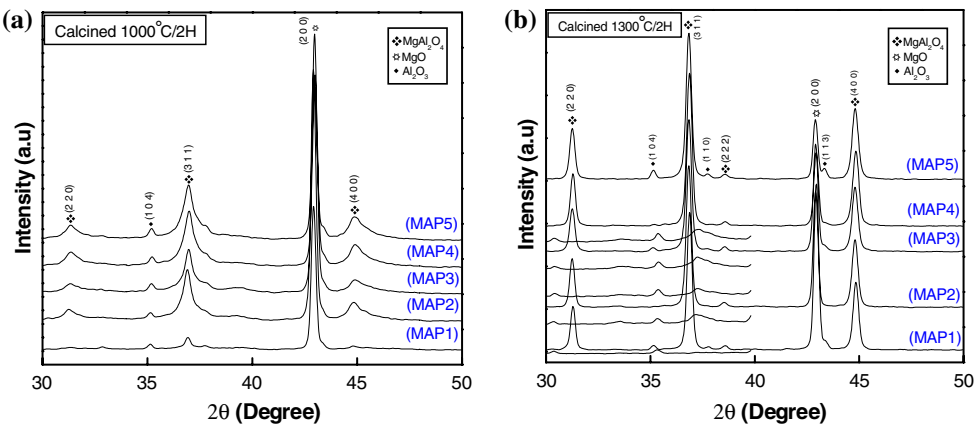

Fig. 1 XRD pattern of Al_2O_3:xMgO (where x = 1, 1.1, 1.2, 1.3 and 1.4 wt.%) powder calcined at (**a**) 1,000 °C/2 h and (**b**) 1,300 °C/2 h

Table 1 The calculated vol% of spinel content of calcined powders obtained from mixture of Al_2O_3:xMgO (where, x = 1:1, 1:1.1, 1:1.2, 1:1.3, 1:1.4 in wt.%)

Identification	Al_2O_3:MgO	vol% of $MgAl_2O_4$ formation after calcination at;			
		1,000(°C)	1,100(°C)	1,200(°C)	1,300(°C)
MAP1	01:01.0	5.59	7.79	26.2	27.58
MAP2	01:01.1	12.23	24.17	33.2	43.97
MAP3	01:01.2	14.33	26.09	34.86	46.52
MAP4	01:01.3	18.59	38.38	46.3	48.37
MAP5	01:01.4	30.32	40.65	48.27	48.26

Table 2 Average crystallite size of spinel phase after calcination of mixed powders at different temperatures

Identification	Al_2O_3:MgO	Calcination temperature (°C)	
		1,000 crystal size (nm)	1,300 crystal size (nm)
MAP1	1:1	19.87	29.87
MAP2	1:1.1	22.80	31.91
MAP3	1:1.2	25.96	32.18
MAP4	1:1.3	26.80	32.32
MAP5	1:1.4	27.11	33.01

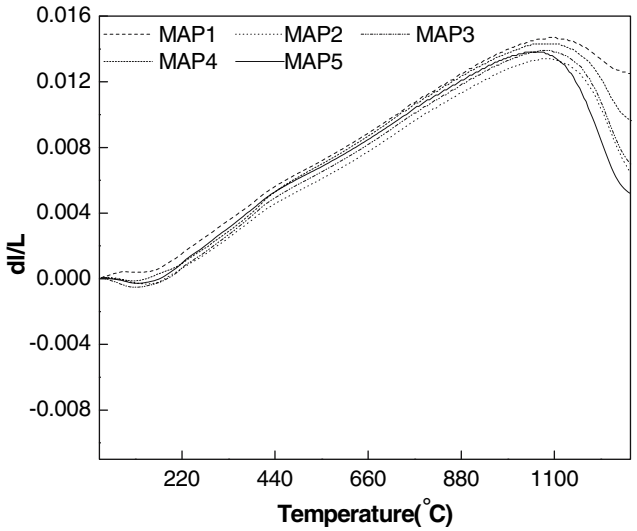

Fig. 2 Dilatometric study of green bar specimen obtained from 1,000 °C/2 h calcined powders

Figure 2 exhibits the dilatometric study of the compacted specimens up to 1,250 °C without any isothermal treatment. The bar (5 × 5 × 15 mm) specimens were prepared after calcination of mixtures of MgO and Al_2O_3 oxides at 1,000 °C for 2 h. An increase in linear expansion up to 1,000 °C in all the batches indicates the starting temperature of spinel formation, which supports the phase analysis obtained from Fig 1a. The percentage linear change beyond 1,000 °C is the combined effect of spinel formation (expansion) and densification (shrinkage). In Fig. 2, MAP5 depicts sharp fall in slope, which implies better sinterability. The presence of inherent oxygen vacancy in magnesia rich spinel composition helps the transport of oxygen ion (the rate controlling factor), resulting in greater extent of amphoteric diffusion, greater mass transport and densification [18]. The slope of MAP5 falls beyond 1,000 °C is due to the exceeding densification rate over the rate of spinel formation.

Figure 3 shows the XRD patterns of sintered samples. There is no evidence of corundum phase in all the different batches, which confirms the consumption of Al_2O_3 in formation of spinel phase, and excess MgO remained as free periclase phase The major phases observed after sintering process in all the batches were that of $MgAl_2O_4$ (311) (220) (400) and MgO (200). The extent of spinel formation has been calculated from the XRD analysis and tabulated in Table 3. However, the total amount of spinel content of sintered specimen is low for MAS5 composition. Highest spinel phase formation in sintered specimen is observed in presence of ~5 vol% seed content in green pellets, and a gradual decreasing trend could be observed with increasing initial seed content. In presence of in-situ 5 vol% spinel seed spinellisation reaches ~70 vol% for MAS1 at 1,600 °C for 4 h through nucleation and growth process, whereas this content reduces to ~62 vol% with increasing temperature when initial seed content was ~28 vol%. However, with increasing MgO content, the extent of spinel phase formation decreases and reaches upto ~50 vol%. Hence, an optimum amount of seed has significant effect on formation of MgO-rich spinel composite. This may be attributed to the effect of the content of spinel crystal seeds, which act as the substrate for heterogeneous nucleation. The rate of nucleation in a unit area of substrate is temperature dependent, which can be expressed as [19]:

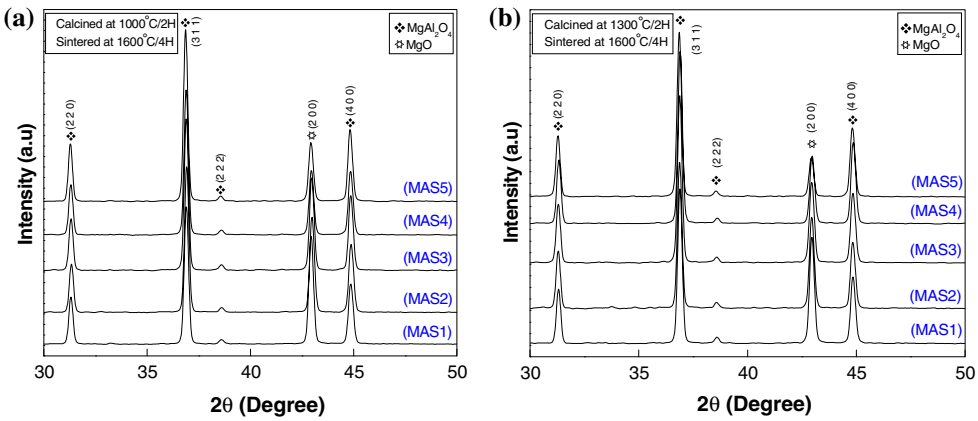

Fig. 3 XRD of sintered specimens of Al_2O_3: xMgO (where x = 1,1.1,1.2,1.3 and 1.4), (**a**) powder calcined at 1,000 °C/2 h and sintered at 1,600 °C/4 h and (**b**) powder calcined at 1,300 °C/2 h and sintered at 1,600 °C/4 h

Table 3 Spinel and MgO phase after sintering (1,600 °C/4 h) of compacts obtained from calcined powders

Identification	Al_2O_3:MgO	vol% $MgAl_2O_4$ content sintered at 1,600 °C		vol% MgO content sintered at 1,600 °C	
		calcinated at			
		1,000(°C)	1,300(°C)	1,000(°C)	1,300(°C)
xMAS1	1.1.0	70.54	62.36	28.12	37.64
MAS2	01:01.1	67.92	60.81	32.07	38.45
MAS3	01:01.2	65.16	58.74	34.14	40.25
MAS4	01:01.3	59.25	52.29	38.80	47.10
MAS5	01:01.4	55.49	49.56	40.74	50.03

$$I^h = K^h \exp\left[-\frac{\Delta G^h_k}{kT}\right] \quad (5)$$

where, I^h is the rate of nucleation in a unit area of substrate, K^h a constant irrespective of the substrate, k is Boltzman constant, T temperature and $\Delta G^h{}_k$ is the potential barrier for heterogeneous nucleation, which can be expressed as:

$$\Delta G^h_4 = \Delta G_k \left[1/4\ ((\ 2 + \cos\theta)\ (\ 1 - \cos\theta\ )^2\ )\right] \quad (6)$$

where, ΔG_k is the potential barrier for homogeneous nucleation, and θ is the contact angle between the crystal nuclei and the substrate. When the substrate is identical to the nucleating crystal, $\theta = 0$ and consequently $\Delta G^h{}_k = 0$, i.e., the potential barrier to nucleation does not exist. However, significant differences exist between the substrate and the nucleating crystal, i.e., $\theta = 180$, $\Delta G^h{}_k = \Delta G_k$, hence, they cannot interact and therefore no acceleration of the nucleation can occur. Using this theory it can be suggested that optimum amount of $MgAl_2O_4$ crystal seeds could decrease the potential barrier for nucleation and therefore accelerate nucleation and growth of the final product ($MgAl_2O_4$) with low seed content. On the other side, the presence of excess seed accelerates the grain growth at high temperature rather than any nucleation effect. Hence, higher percentages of seed have not any advantages on the further spinel formation.

The relative density of different sintered samples was measured. Figure 4 exhibits a slight but gradual increase in density of MAS1 upto addition of 26 vol% spinel seed, however, the trend become reverse with increasing calcination temperature as well as seed content. Tables 1 and 3 reveals that the spinel content of the sintered specimen can be controlled by the initial calcination temperature of the mixture of starting materials. The characteristic curve of both the specimen (MAS1 and MAS5) illustrates the higher content of spinel seed has deleterious effect on densification behavior. An increase in trend of density may be associated with better sintering of the body due to the

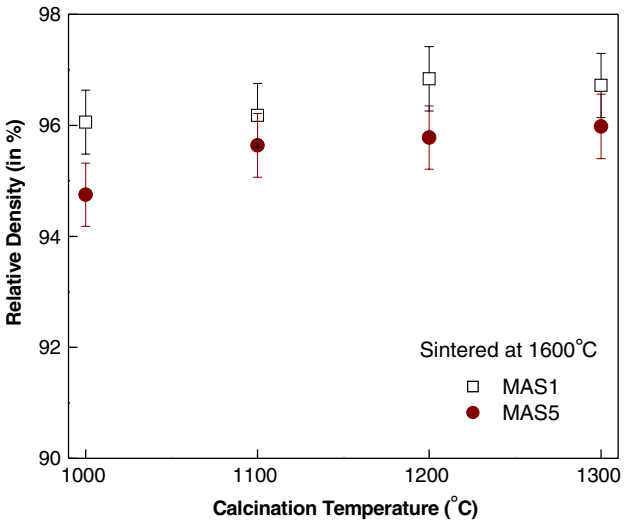

Fig. 4 Relative density of sintered samples calcined at various temperatures and sintered at 1,600 °C

presence of reactive spinel phase with average crystallite size of 19–30 nm and proper densification of the body in between MgO grains by finer spinel phase as observed in Fig. 5. High temperature calcined (1,300 °C) materials exhibit a low value of relative density due to the coarsening effect and this is presumably higher content of spinel favors more diffusion and favors grain growth. The comparatively coarser particles densify intensely, but, particle size much finer to a certain critical value is of no benefit for densification [20]. Very coarse materials reveal the poor density, which has obeyed the general conditions of sintering. In case of MAS1 and MAS5, the coarsening is predominant rather than diffusion due to presence of more than 26 vol% spinel content. When the seed content is 30 vol% the volume expansion is predominant and hence the reduced relative density. The relative density varies between 96% and 98% for MAS1, whereas MAS5 exhibits this variation within the range of 95–97%. However, the densification study does not show any significant difference

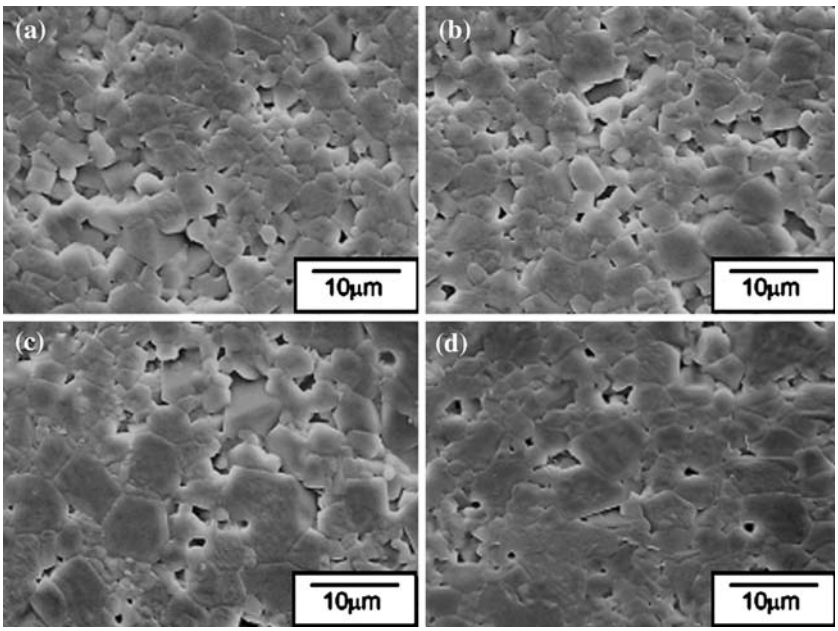

Fig. 5 SEM image of (**a**) MAP1 powder calcined at 1,000 °C & sintered at 1,600 °C/4 h (**b**) MAP1 powder calcined at 1,300 °C & sintered at 1,600 °C/4 h (**c**) MAP5 powder calcined at1,000 °C & sintered at 1,600 °C/4 h (**d**) MAP5 powder calcined at1,300°C & sintered at 1,600 °C/4 h

among the batches, which may be due to the similar true density values for both spinel and periclase phases.

Nearly 96% relative densification is exhibited for highest MgO containing (MAS5) specimen when constituent powder was calcined at 1,300 °C for 2 h and followed by sintering at 1,600 °C for 4 h. The densification process is greatly influenced by calcination process, and the presence of free periclase hinders the grain boundary migration. Figure 5a and b represents the microstructure of MAS1 specimen, which are calcined at different temperature and sintered at 1,600 °C/4 h (Fig. 6). Micrograph reveals the average grain size of MAP1 calcined at 1,300 °C is ~8 μm

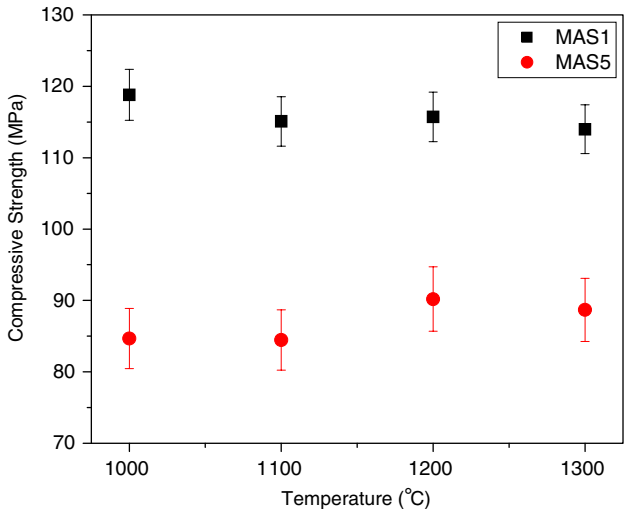

Fig. 6 Compressive Strength (σ_{comp}) of MAS1 and MAS5 as a function of temperature. The sintering was carried out at 1,600 °C/4 h

in comparison to MAP1 calcined at 1,000 °C. Similarly, Figure 5c and d exhibits the microstructure of MAS5 with relatively larger and elongated grain at around ~9 and 16 μm, when specimens were sintered after calcination at 1,000 °C and 1,300 °C temperature respectively. Direct-bonded and rounded spinel–spinel grains with relatively few edges are also observed. Figure 5a reveals that grains of MAS1 are non-uniform and pores (intergranular) are present in between the grains. The average grain size was observed to be ~5 μm. Excess MgO suppresses the grain growth. However, some large grains could be noticed in Fig 5b, where content of crystal seed is ~30 vol%. Figure 5d illustrates the microstructure of sample MAS5 appear to be denser with fewer pores, which confirm the results of densification parameter. The grains in samples MAS5 seem to appear as layered grains. Abnormal grain growth was identified when the powders calcined at 1,300 °C and sintered at 1,600 °C for 4 h. Random grain orientation and increased intergranular porosity is responsible to deteriorate the density of MAS5 specimen. From the microstructure, the average grain size ~5 μm of MAS1 calcined at 1,000 °C and sintered at 1,600 °C/4 h may exhibit improved room temperature mechanical properties, whereas MAS5, calcined at 1,300 °C and sintered at 1,600 °C/4 h is expected to provide better high temperature mechanical properties because of elongated and larger grain size.

The mechanical properties of MgO-spinel composites containing preformed spinel are more strongly influenced than the in-situ formed spinel composites by sintering temperature, volume fraction and particle size of spinel [9]. The evaluation of compressive strength of spinel-based

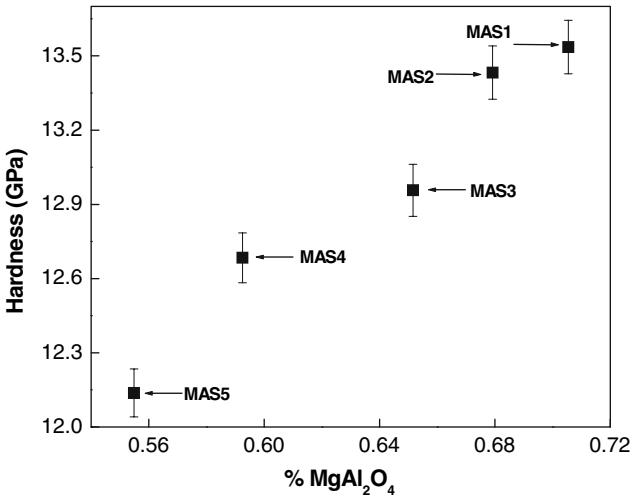

Fig. 7 Hardness of various sintered specimen as a function of increasing spinel content for sintered compacts obtained from powder calcined at 1,000 °C/2 h and sintered at 1,600 °C/4 h

refractory has significant effect under loading [10]. The compressive strength of both of the MAS1 and MAS5 specimens does not have significant change with respect to preformed spinel addition and/or calcination temperature. Around 20% fall in strength could be noticed for MAS5, this is presumably due to: (a) the excessive grain growth of spinel phase during sintering and (b) the low bond strength within preformed spinel grain and MgO. MgO-Spinel composites with α_{spinel} (7.6 MK^{-1}) < α_{MgO} (13.5 MK^{-1}) show low strength in comparison with pure MgO, because the thermal expansion mismatch leads to large tensile hoop stresses and microcrack development around the spinel grains, and the radial cracks produced readily link together [9]. These cracks are the critical defects causing failure on loading. Hardness of the studied materials may be explained on the basis of the grain size and morphology. Vickers Hardness of sinter samples at different concentration of spinel is shown in Fig. 7. Figure 8 reveals the hardness of the MgO-Spinel composite (MAS1) is ~13.5 GPa, which continuously decreases (13.7–12.1 GPa) with the content of spinel phase at sintered specimen. Higher amount of seed addition has an adverse affect on the hardness of the composites due to coarsening of the spinel grains and formation of subsequent porosity. It has also been noticed that these composite materials also obey Hall–Petch relationship [21, 22]. The present study shows that the average particle size has significant impact on mechanical properties, which is controlled by spinel seed content and initial calcination temperature.

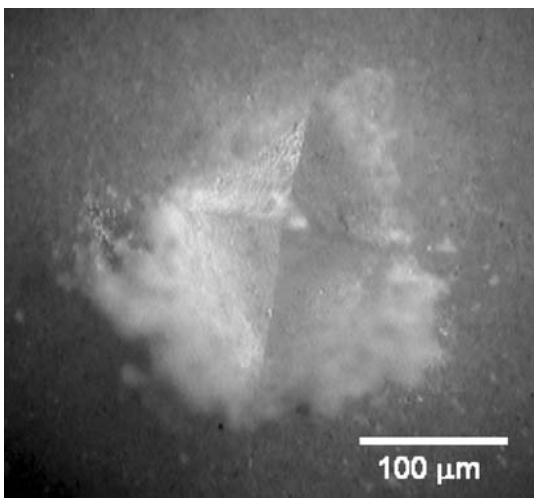

Fig. 8 Optical Image of indentation shape of MAS1 (Al_2O_3: MgO = 1:1) at load of 98N

Conclusions

Initial calcination temperature and in-situ formation of spinel phase have significant contribution on the composition and microstructure of sintered composite. Around 5 vol% spinel seed is effective for the synthesis of MgO-70 vol% $MgAl_2O_4$, whereas MgO-50 vol% $MgAl_2O_4$ composite can be synthesized in presence of ~50 vol% initial seed content. Higher content of seed has no contribution to nucleation rather it accelerates the grain growth at high temperature. This growth of grain size is detrimental for mechanical properties. By adjusting the level of spinel phase in the green pellets and the sintering conditions, the physical properties can be synchronized.

References

1. Bartha P (1989) In: Zhong X et al (ed) Proc. Int. Symp. Refractories, Refractory Raw Materials and High Performance Refractory Products, Pergamon, Hangzhou, pp 661–674
2. Reyes Sanchez JA, Toledo OD (1989) New Developments of magnesite-chrome brick and magnesite-spinel for cement rotary kilns-higher thermal shock resistance and higher coating adherence. In UNITECR 1989 CONGRESS, Anaheim, USA, p 968
3. Dal Maschio R, Fabbri B, Fiori C (1988) Ind Ceram 8(3):121
4. Gonsalves GE, Duarte AK, Brant PORC (1993) Am Ceram Soc Bull 72(2):49
5. Bailey JT, Russel R (1971) Am Ceram Soc Bull 50(5):493
6. Pasquier JF, Komarneni S, Roy R (1991) J Mat Sci 26:3797
7. Ghosh A, Sarkar R, Mukherjee B, Das SK (2004) J Eu Ceram Soc 24:2079
8. Cooper SC, Hudson TA (1982) Trans & J Br Ceram Soc 81(4):121
9. Aksel C, Rand B, Riley FL, Warren PD (2002) J Eu Ceram Soc 22:745
10. Simonov KV, Koksharov VD, Zabotka AI, Reinov LA (1983) Ogneupory 1:7
11. Huang C, Lu T, Lin L, Lei M, Huang C (2007) Key Eng Mat 336–338:1207–1210

12. Domanski D, Urettavizcaya G, Castro FJ, Gennari FC (2004) J Am Ceram Soc 87(11):2020
13. Cullity BD (1978) Elements of X-Ray Diffraction, 2nd ed. p 351
14. Procopio AT, Zavaliangos A, Cunningham JC (2003) J Mat Sci 38:3629
15. Barsoum MW (1997) Fundamentals of ceramics. McGRAW-HILL International Editions
16. Zawrah MF (2004) Mat Sci Eng A 382:362
17. Matsui M, Takashi T, Oda I (1984) In: Kingery WD (ed) Advances in ceramics, vol 10. The American Ceramic Society, Columbus, OH, p 562
18. Kenya H, Tadashi O, Zenbee N (1977) Rep Res Lab Eng Mater, Tokyo Institute of Technology, No. 2, p 85
19. Kingery WD, Bowen HK, Uhlmann DR (1991) Introduction of ceramics, 2nd edn. John Wiley & Sons, p 335
20. Petkovic J, Ristic MM (1973) Ceramurgia 3(1):12
21. Hall EO (1951) Proc Phys Soc (Lond) B64:747
22. Petch NJ (1953) J Iron Steel Inst 174:25